Draft version November 17, 2015
Preprint typeset using LaTeX style emulateapj v. 01/23/15

SUPERMASSIVE BLACK HOLES AND THEIR HOST SPHEROIDS III. MBH-N PAPER

G. A. D. Savorgnan[1]
Centre for Astrophysics and Supercomputing, Swinburne University of Technology, Hawthorn, Victoria 3122, Australia.
Draft version November 17, 2015

ABSTRACT

The Sérsic $R^{1/n}$ model is the best approximation known to date for describing the light distribution of stellar spheroidal and disk components, with the Sérsic index n providing a direct measure of the central radial concentration of stars. The Sérsic index of a galaxy's spheroidal component, $n_{\rm sph}$, has been shown to tightly correlate with the mass of the central supermassive black hole, $M_{\rm BH}$. The $M_{\rm BH}-n_{\rm sph}$ correlation is also expected from other two well known scaling relations: the $L_{\rm sph}-n_{\rm sph}$ and the $M_{\rm BH}-L_{\rm sph}$, where $L_{\rm sph}$ indicates the galaxy's spheroid luminosity. However, it is widely recognized that obtaining an accurate estimate of the spheroid Sérsic index is a challenging task, and – not surprisingly – some studies have failed to recover a statistically significant $M_{\rm BH}-n_{\rm sph}$ correlation. With the aim of re-investigating the $M_{\rm BH}-n_{\rm sph}$ and other black hole mass scaling relations, we performed a detailed (i.e. bulge, disks, bars, spiral arms, rings, halo, nucleus, etc.) decomposition of 66 galaxies, with directly measured black hole masses, that had been imaged at 3.6 μm with *Spitzer*. In this paper, the third of its series, we present an analysis of the $L_{\rm sph}-n_{\rm sph}$ and $M_{\rm BH}-n_{\rm sph}$ diagrams. While early-type (elliptical+lenticular) and late-type (spiral) galaxies split into two separate relations in the $L_{\rm sph}-n_{\rm sph}$ and $M_{\rm BH}-L_{\rm sph}$ diagrams, they reunite in a single $M_{\rm BH}\propto n_{\rm sph}^{3.39\pm0.15}$ sequence with relatively small intrinsic scatter ($\epsilon_{(Y|X)}\simeq0.25$ dex). **to be finished...**

Subject headings: keywords

1. INTRODUCTION

The empirical Sérsic (1963, 1968) $R^{1/n}$ model has been demonstrated to provide adequate description of the light distribution of the stellar spheroidal[1] and disk components of galaxies (e.g. Caon et al. 1993; Andredakis et al. 1995; Iodice et al. 1997, 1999; Seigar & James 1998; Khosroshahi et al. 2000), yet its physical origin has remained unexplained for decades. The Sérsic model parametrizes the intensity of light I as a function of the projected galactic radius R such that

$$I(R;I_{\rm e},R_{\rm e},n)=I_{\rm e}\exp\left\{-b_{\rm n}\left[\left(\frac{R}{R_{\rm e}}\right)^{1/n}-1\right]\right\},$$

where $I_{\rm e}$ indicates the intensity at the effective radius $R_{\rm e}$ that encloses half of the total light from the model, the Sérsic index n is the parameter that regulates the curvature of the radial light profile, and $b_{\rm n}$ is a constant defined in terms of the Sérsic index n (see Graham & Driver 2005, and references therein). A large Sérsic index corresponds to a steep inner profile and a shallow outer profile, whereas a small Sérsic index corresponds to a shallow inner profile and a steep outer profile. This means that, for a stellar spheroidal system whose light distribution is well approximated by the Sérsic model, the larger the Sérsic index is, the more centrally concentrated the stars are and the more extended the outer envelope is.

A compelling physical interpretation for the Sérsic profile family was recently theorized by Cen (2014) and later confirmed by Nipoti (2015) by means of N-body simulations. Cen (2014) conjectured that, when structures form within a standard cold dark matter model seeded by random Gaussian fluctuations, any centrally concentrated stellar structure always possesses an extended stellar envelope, and vice versa. Nipoti (2015) quantitatively explored Cen's hypothesis and showed that systems originated from several mergers have a large Sérsic index ($n\gtrsim4$), whereas systems with a Sérsic index as small as $n\simeq2$ can be produced by coherent dissipationless collapse, and exponential profiles ($n=1$) can only be obtained through dissipative processes. This scenario sets the theoretical framework for the well known correlation between the spheroid luminosity, $L_{\rm sph}$, and the spheroid Sérsic index, $n_{\rm sph}$, (e.g. Young & Currie 1994; Jerjen et al. 2000; Graham & Guzmán 2003), although the numerical results of Nipoti (2015) seem to lack of spheroidal systems with Sérsic indices as large as $7-10$, which are commonly observed in the local Universe.

Given the existence of the $L_{\rm sph}-n_{\rm sph}$ correlation and the relation between the central black hole mass, $M_{\rm BH}$, and the spheroid luminosity (e.g. Magorrian et al. 1998), an $M_{\rm BH}-n_{\rm sph}$ relation must exist. After Graham (2001) showed that the black hole mass is tightly linked to the stellar light concentration of spheroids (measured through a parameter different from, but closely related to the Sérsic index), Graham & Driver (2007) presented for the first time the $M_{\rm BH}-n_{\rm sph}$ correlation using a sample of 27 elliptical and disk galaxies. Graham & Driver (2007) fit their data with a log-quadratic regression, finding that the $M_{\rm BH}-n_{\rm sph}$ log-relation is steeper for spheroids with small Sérsic indices and shallower for spheroids with large Sérsic indices, and measured a rel-

gsavorgn@astro.swin.edu.au

[1] Throughout the text, we use the term "spheroid" to designate either a diskless elliptical galaxy or the bulge component of a disk galaxy, with no attempt at distinguishing between classical bulges and disk-like pseudo-bulges.

atively small level of scatter[2]. A few years later, Sani et al. (2011), Vika et al. (2012) and Beifiori et al. (2012) performed multi-component decompositions for samples of galaxies similar to that used by Graham & Driver (2007), but they unexpectedly failed to recover a strong $M_{\rm BH}-n_{\rm sph}$ relation. This issue was tackled by Savorgnan et al. (2013), who collected the Sérsic index measurements published by Graham & Driver (2007), Sani et al. (2011), Vika et al. (2012) and Beifiori et al. (2012) for a sample of 54 galaxies, and showed that, by rejecting the most discrepant measurements and averaging the remaning ones, a strong $M_{\rm BH}-n_{\rm sph}$ relation was retrieved. Remarkably, Savorgnan et al. (2013) repeated their analysis upon excluding the Sérsic index measurements of Graham & Driver (2007) and still regained a significant $M_{\rm BH}-n_{\rm sph}$ relation. This was suggesting that the individual galaxy decompositions of Sani et al. (2011), Vika et al. (2012) and Beifiori et al. (2012) were not accurate, i.e. each individual study obtained "noisy" Sérsic index measurements which prevented the recovery of a strong $M_{\rm BH}-n_{\rm sph}$ relation.

Motivated by the need of more accurate galaxy decompositions to refine and re-investigate scaling relations between the black hole mass and several galaxy structural parameters, we performed state-of-the-art modelling for the largest sample of galaxies to date (Savorgnan & Graham 2015a, hereafter *Paper I*), for which a dynamical measurement of the black hole mass was available. In doing so, we used 3.6 μm *Spitzer* satellite imagery, given its superb capability to trace the stellar mass (Sheth et al. 2010, and references therein). In Savorgnan et al. (2015, hereafter *Paper II*) we examined the correlations between the black hole mass and the total galaxy luminosity, the spheroid luminosity and the spheroid stellar mass. Here we focus on the $M_{\rm BH}-n_{\rm sph}$ relation.

This paper (*Paper III*) is structured as follows...

2. DATA

We populated the $L_{\rm sph}-n_{\rm sph}$ and $M_{\rm BH}-n_{\rm sph}$ diagrams with the same galaxy sample used in *Paper II* (and presented here in Table 1), i.e. 66 galaxies for which a dynamical measurement of the black hole mass has been reported in the literature (by Graham & Scott 2013 or Rusli et al. 2013) and for which we were able to successfully model the light distribution and measure the spheroid structural parameters using 3.6 μm *Spitzer* satellite images. Our galaxy decompositions take into account bulge, disks, spiral arms, bars, rings, halo, extended or unresolved nuclear source and partially depleted core, and – for the first time – they were checked to be consistent with the galaxy kinematics (Emsellem et al. 2011; Scott et al. 2014; Arnold et al. 2014). Kinematical information was used to confirm the presence of disk components in the majority of early-type (elliptical + lenticular) galaxies and, more importantly, to estabilish the radial extent of these disks, which in most cases is not obvious from a visual inspection of the galaxy images. This enabled us to distinguish between intermediate-scale disks, that are fully embedded in the spheroid, and large-scale disks, that encase the bulge and dominate the light at large radii. Savorgnan & Graham (2015b) demonstrate that when an intermediate-scale disk is misclassified and modeled as a large-scale disk, the luminosity of the spheroid is underestimated, hence the galaxy incorrectly appears as a positive outlier (an "over-massive" black hole) in the $M_{\rm BH}-L_{\rm sph}$ diagram. A detailed description of the dataset used here, the data reduction process and the galaxy modelling technique that we developed can be found in *Paper I*, along with a discussion of how we estimated the uncertainties on the spheroid Sérsic indices[3]. The morphological classification (E = elliptical; E/S0 = elliptical/lenticular; S0 = lenticular; S0/Sp = lenticular/spiral; Sp = spiral; and "merger") follows from the galaxy decompositions illustrated in *Paper I*. As in *Paper II*, we will refer to early-type galaxies (E+S0) and late-type galaxies (Sp). The early-type bin includes the two galaxies classified as E/S0, whereas the two galaxies classified as S0/Sp and the two galaxies classified as mergers are included in neither the early- nor the late-type bin.

3. ANALYSIS AND RESULTS

As in *Paper II*, a linear regression analysis of the $L_{\rm sph}-n_{\rm sph}$ (Table 3 and Figure 1) and $M_{\rm BH}-n_{\rm sph}$ (Table 4 and Figure 2) diagrams was performed using three different routines: the BCES code from Akritas & Bershady (1996), the FITEXY routine (Press et al. 1992), as modified by Tremaine et al. (2002), and the Bayesian estimator `linmix_err` (Kelly 2007). All of these three routines take into account the intrinsic scatter, but only the FITEXY and the `linmix_err` codes allow one to quantify it. We report both symmetrical and nonsymmetrical linear regressions. Symmetrical regressions are meant to be compared with theoretical expectations, whereas nonsymmetrical forward $(Y|X)$ regressions – which minimize the scatter in the Y direction – allow one to predict the value of the observable Y with the best possible precision.

We searched for extreme outliers in both the $L_{\rm sph}-n_{\rm sph}$ and $M_{\rm BH}-n_{\rm sph}$ diagrams, and found that in our $L_{\rm sph}-n_{\rm sph}$ plot there are no 3σ outliers, whereas in our $M_{\rm BH}-n_{\rm sph}$ plot the lenticular galaxies NGC 0524 and NGC 3998 reside more than 3σ from the bisector linear regression for all galaxies. These two galaxies have therefore been excluded from the rest of the analysis.

3.1. $L_{\rm sph}-n_{\rm sph}$

Following Graham (2001), who showed that the $L_{\rm sph}-n_{\rm sph}$ relation is different for elliptical galaxies and the bulges of disk galaxies (S0+Sp), Savorgnan et al. (2013) re-analyzed the data from Graham & Guzmán (2003) and Graham & Worley (2008) and obtained two separate $L_{\rm sph}-n_{\rm sph}$ linear regressions for elliptical galaxies and the bulges of disk galaxies (in the B- and K-band, respectively). At the time, the $L_{\rm sph}-n_{\rm sph}$ datasets from Graham & Guzmán (2003) and Graham & Worley

[2] At the time, the $M_{\rm BH}-\sigma$ relation (Ferrarese & Merritt 2000; Gebhardt et al. 2000) was reported to have the same level of scatter as the $M_{\rm BH}-n_{\rm sph}$ relation ($\simeq 0.3$ dex).

[3] The uncertainties associated with the spheroid Sérsic indices were estimated with a method that takes into account systematic errors. This method consists in comparing, for each of our galaxies, the measurements of the spheroid Sérsic index obtained by different studies with that obtained by us. Systematic errors are typically not considered by popular 2D fitting codes, which report only the statistical errors associated with their fitted parameters. Readers should refer to *Paper I* for a more detailed discussion on this topic.

TABLE 1
GALAXY SAMPLE.

Galaxy	**Type**	**Distance**	$M_{\mathbf{BH}}$	$MAG_{\mathbf{sph}}$	$n^{\mathbf{maj}}_{\mathbf{sph}}$
		[Mpc]	[10^8 $M_\odot$]	[mag]	
(1)	(2)	(3)	(4)	(5)	(6)
IC 1459	E	28.4	24^{+10}_{-10}	$-26.15^{+0.18}_{-0.11}$	$6.6^{+0.9}_{-0.8}$
IC 2560	Sp (bar)	40.7	$0.044^{+0.044}_{-0.022}$	$-22.27^{+0.66}_{-0.58}$	$0.8^{+0.4}_{-0.3}$
IC 4296	E	40.7	11^{+2}_{-2}	$-26.35^{+0.18}_{-0.11}$	$5.8^{+0.8}_{-0.7}$
M31	Sp (bar)	0.7	$1.4^{+0.9}_{-0.3}$	$-22.74^{+0.18}_{-0.11}$	$2.2^{+0.3}_{-0.3}$
M49	E	17.1	25^{+3}_{-1}	$-26.54^{+0.18}_{-0.11}$	$6.6^{+0.9}_{-0.8}$
M59	E	17.8	$3.9^{+0.4}_{-0.4}$	$-25.18^{+0.18}_{-0.11}$	$5.5^{+0.8}_{-0.7}$
M64	Sp	7.3	$0.016^{+0.004}_{-0.004}$	$-21.54^{+0.18}_{-0.11}$	$0.8^{+0.1}_{-0.1}$
M81	Sp (bar)	3.8	$0.74^{+0.21}_{-0.11}$	$-23.01^{+0.88}_{-0.66}$	$1.7^{+1.3}_{-0.7}$
M84	E	17.9	$9.0^{+0.9}_{-0.8}$	$-26.01^{+0.66}_{-0.58}$	$7.8^{+3.6}_{-2.5}$
M87	E	15.6	$58.0^{+3.5}_{-3.5}$	$-26.00^{+0.66}_{-0.58}$	$10.0^{+4.7}_{-3.2}$
M89	E	14.9	$4.7^{+0.5}_{-0.5}$	$-24.48^{+0.66}_{-0.58}$	$4.6^{+2.2}_{-1.5}$
M94	Sp (bar)	4.4	$0.060^{+0.014}_{-0.014}$	$-22.08^{+0.18}_{-0.11}$	$0.9^{+0.1}_{-0.1}$
M96	Sp (bar)	10.1	$0.073^{+0.015}_{-0.015}$	$-22.15^{+0.18}_{-0.11}$	$1.5^{+0.2}_{-0.2}$
M104	S0/Sp	9.5	$6.4^{+0.4}_{-0.4}$	$-23.91^{+0.66}_{-0.58}$	$5.8^{+2.7}_{-1.8}$
M105	E	10.3	4^{+1}_{-1}	$-24.29^{+0.66}_{-0.58}$	$5.2^{+2.4}_{-1.6}$
M106	Sp (bar)	7.2	$0.39^{+0.01}_{-0.01}$	$-21.11^{+0.18}_{-0.11}$	$2.0^{+0.3}_{-0.2}$
NGC 0524	S0	23.3	$8.3^{+2.7}_{-1.3}$	$-23.19^{+0.18}_{-0.11}$	$1.1^{+0.2}_{-0.1}$
NGC 0821	E	23.4	$0.39^{+0.26}_{-0.09}$	$-24.00^{+0.88}_{-0.66}$	$5.3^{+4.1}_{-2.3}$
NGC 1023	S0 (bar)	11.1	$0.42^{+0.04}_{-0.04}$	$-22.82^{+0.18}_{-0.11}$	$2.1^{+0.3}_{-0.3}$
NGC 1300	Sp (bar)	20.7	$0.73^{+0.69}_{-0.35}$	$-22.06^{+0.66}_{-0.58}$	$3.8^{+1.8}_{-1.2}$
NGC 1316	merger	18.6	$1.50^{+0.75}_{-0.80}$	$-24.89^{+0.66}_{-0.58}$	$2.0^{+1.0}_{-0.7}$
NGC 1332	E/S0	22.3	14^{+2}_{-2}	$-24.89^{+0.88}_{-0.66}$	$5.1^{+3.9}_{-2.2}$
NGC 1374	E	19.2	$5.8^{+0.5}_{-0.5}$	$-23.68^{+0.18}_{-0.11}$	$3.7^{+0.5}_{-0.5}$
NGC 1399	E	19.4	$4.7^{+0.6}_{-0.6}$	$-26.43^{+0.18}_{-0.11}$	$10.0^{+1.4}_{-1.2}$
NGC 2273	Sp (bar)	28.5	$0.083^{+0.004}_{-0.004}$	$-23.00^{+0.66}_{-0.58}$	$2.1^{+1.0}_{-0.7}$
NGC 2549	S0 (bar)	12.3	$0.14^{+0.02}_{-0.13}$	$-21.25^{+0.18}_{-0.11}$	$2.3^{+0.3}_{-0.3}$
NGC 2778	S0 (bar)	22.3	$0.15^{+0.09}_{-0.10}$	$-20.80^{+0.66}_{-0.58}$	$1.3^{+0.6}_{-0.4}$
NGC 2787	S0 (bar)	7.3	$0.40^{+0.04}_{-0.05}$	$-20.11^{+0.66}_{-0.58}$	$1.1^{+0.5}_{-0.4}$
NGC 2974	Sp (bar)	20.9	$1.7^{+0.2}_{-0.2}$	$-22.95^{+0.66}_{-0.58}$	$1.4^{+0.7}_{-0.5}$
NGC 3079	Sp (bar)	20.7	$0.024^{+0.024}_{-0.012}$	$-23.01^{+0.66}_{-0.58}$	$1.3^{+0.6}_{-0.4}$
NGC 3091	E	51.2	36^{+1}_{-2}	$-26.28^{+0.18}_{-0.11}$	$7.6^{+1.0}_{-0.9}$
NGC 3115	E/S0	9.4	$8.8^{+10.0}_{-2.7}$	$-24.22^{+0.18}_{-0.11}$	$4.4^{+0.6}_{-0.5}$
NGC 3227	Sp (bar)	20.3	$0.14^{+0.10}_{-0.06}$	$-21.76^{+0.66}_{-0.58}$	$1.7^{+0.8}_{-0.5}$
NGC 3245	S0 (bar)	20.3	$2.0^{+0.5}_{-0.5}$	$-22.43^{+0.18}_{-0.11}$	$2.9^{+0.4}_{-0.3}$
NGC 3377	E	10.9	$0.77^{+0.04}_{-0.06}$	$-23.49^{+0.66}_{-0.58}$	$7.7^{+3.6}_{-2.5}$
NGC 3384	S0 (bar)	11.3	$0.17^{+0.01}_{-0.02}$	$-22.43^{+0.18}_{-0.11}$	$1.6^{+0.2}_{-0.2}$
NGC 3393	Sp (bar)	55.2	$0.34^{+0.02}_{-0.02}$	$-23.48^{+0.66}_{-0.58}$	$3.4^{+1.6}_{-1.1}$
NGC 3414	E	24.5	$2.4^{+0.3}_{-0.3}$	$-24.35^{+0.18}_{-0.11}$	$4.8^{+0.7}_{-0.6}$
NGC 3489	S0/Sp (bar)	11.7	$0.058^{+0.008}_{-0.008}$	$-21.13^{+0.66}_{-0.58}$	$1.5^{+0.7}_{-0.5}$
NGC 3585	E	19.5	$3.1^{+1.4}_{-0.6}$	$-25.52^{+0.66}_{-0.58}$	$5.2^{+2.4}_{-1.7}$
NGC 3607	E	22.2	$1.3^{+0.5}_{-0.5}$	$-25.36^{+0.66}_{-0.58}$	$5.5^{+2.6}_{-1.7}$
NGC 3608	E	22.3	$2.0^{+1.1}_{-0.6}$	$-24.50^{+0.66}_{-0.58}$	$5.2^{+2.4}_{-1.7}$
NGC 3842	E	98.4	97^{+30}_{-26}	$-27.00^{+0.18}_{-0.11}$	$8.1^{+1.1}_{-1.0}$
NGC 3998	S0 (bar)	13.7	$8.1^{+2.0}_{-1.9}$	$-22.32^{+0.88}_{-0.66}$	$1.2^{+0.9}_{-0.5}$
NGC 4026	S0 (bar)	13.2	$1.8^{+0.6}_{-0.3}$	$-21.58^{+0.88}_{-0.66}$	$2.4^{+1.8}_{-1.0}$
NGC 4151	Sp (bar)	20.0	$0.65^{+0.07}_{-0.07}$	$-23.40^{+0.66}_{-0.58}$	$1.4^{+0.6}_{-0.4}$
NGC 4261	E	30.8	5^{+1}_{-1}	$-25.72^{+0.66}_{-0.58}$	$4.7^{+2.2}_{-1.5}$
NGC 4291	E	25.5	$3.3^{+0.9}_{-2.5}$	$-24.05^{+0.66}_{-0.58}$	$4.2^{+2.0}_{-1.4}$
NGC 4388	Sp (bar)	17.0	$0.075^{+0.002}_{-0.002}$	$-21.26^{+0.88}_{-0.66}$	$0.6^{+0.5}_{-0.3}$
NGC 4459	S0	15.7	$0.68^{+0.13}_{-0.13}$	$-23.48^{+0.66}_{-0.58}$	$3.1^{+1.5}_{-1.0}$
NGC 4473	E	15.3	$1.2^{+0.4}_{-0.9}$	$-23.88^{+0.66}_{-0.58}$	$2.3^{+1.1}_{-0.7}$
NGC 4564	S0	14.6	$0.60^{+0.03}_{-0.09}$	$-22.30^{+0.18}_{-0.11}$	$2.6^{+0.4}_{-0.3}$
NGC 4596	S0 (bar)	17.0	$0.79^{+0.38}_{-0.33}$	$-22.73^{+0.18}_{-0.11}$	$2.7^{+0.4}_{-0.3}$

Galaxy	**Type**	**Distance**	$M_{\rm BH}$	$MAG_{\rm sph}$	$n_{\rm sph}^{\rm maj}$
		[Mpc]	[10^8 $M_\odot$]	[mag]	
(1)	(2)	(3)	(4)	(5)	(6)
NGC 4697	E	11.4	$1.8^{+0.2}_{-0.1}$	$-24.82^{+0.88}_{-0.66}$	$7.2^{+5.5}_{-3.1}$
NGC 4889	E	103.2	210^{+160}_{-160}	$-27.54^{+0.18}_{-0.11}$	$8.1^{+1.1}_{-1.0}$
NGC 4945	Sp (bar)	3.8	$0.014^{+0.014}_{-0.007}$	$-20.96^{+0.66}_{-0.58}$	$1.4^{+0.7}_{-0.5}$
NGC 5077	E	41.2	$7.4^{+4.7}_{-3.0}$	$-25.45^{+0.18}_{-0.11}$	$4.2^{+0.6}_{-0.5}$
NGC 5128	merger	3.8	$0.45^{+0.17}_{-0.10}$	$-23.89^{+0.88}_{-0.66}$	$1.2^{+0.9}_{-0.5}$
NGC 5576	E	24.8	$1.6^{+0.3}_{-0.4}$	$-24.44^{+0.18}_{-0.11}$	$3.3^{+0.5}_{-0.4}$
NGC 5845	S0	25.2	$2.6^{+0.4}_{-1.5}$	$-22.96^{+0.88}_{-0.66}$	$2.5^{+1.9}_{-1.1}$
NGC 5846	E	24.2	11^{+1}_{-1}	$-25.81^{+0.66}_{-0.58}$	$6.4^{+3.0}_{-2.1}$
NGC 6251	E	104.6	5^{+2}_{-2}	$-26.75^{+0.18}_{-0.11}$	$6.8^{+0.9}_{-0.8}$
NGC 7052	E	66.4	$3.7^{+2.6}_{-1.5}$	$-26.32^{+0.18}_{-0.11}$	$4.2^{+0.6}_{-0.5}$
NGC 7619	E	51.5	25^{+8}_{-3}	$-26.35^{+0.66}_{-0.58}$	$5.3^{+2.5}_{-1.7}$
NGC 7768	E	112.8	13^{+5}_{-4}	$-26.90^{+0.66}_{-0.58}$	$8.4^{+3.9}_{-2.7}$
UGC 03789	Sp (bar)	48.4	$0.108^{+0.005}_{-0.005}$	$-22.77^{+0.88}_{-0.66}$	$1.9^{+1.4}_{-0.8}$

NOTE. — *Column (1)*: Galaxy name. *Column (2)*: Morphological type (E=elliptical, S0=lenticular, Sp=spiral, merger). The morphological classification of four galaxies is uncertain (E/S0 or S0/Sp). The presence of a bar is indicated. *Column (3)*: Distance. *Column (4)*: Black hole mass. *Column (5)*: Absolute 3.6 μm spheroid magnitude. *Column (6)*: Spheroid major-axis Sérsic index. Spheroid magnitudes and Sérsic indices come from our state-of-the-art multicomponent galaxy decompositions (*Paper I*), which include bulges, disks, bars, spiral arms, rings, haloes, extended or unresolved nuclear sources and partially depleted cores, and that – for the first time – were checked to be consistent with the galaxy kinematics. The uncertainties were estimated with a method that takes into account systematic errors, which are typically not considered by popular 2D fitting codes.

(2008) were of the best quality available to investigate the $L_{\rm sph} - n_{\rm sph}$ relation for different galaxy morphological types. However, these datasets were not obtained from a homogeneous analysis, but they were a collection of results taken from various past bulge/disk decomposition studies. Here we re-investigate the $L_{\rm sph} - n_{\rm sph}$ diagram using only our high-quality dataset. Spheroid luminositites and Sérsic indices were obtained from accurate multicomponent decompositions, performed in a consistent manner using the 3.6 μm band, which is less affected by dust extinction than the K-band.

Graham & Worley (2008) presented a single $L_{\rm sph} - n_{\rm sph}$ correlation for the bulges of disk galaxies (S0+Sp). However, using our dataset, we fit the $L_{\rm sph} - n_{\rm sph}$ relation for elliptical, lenticular and spiral galaxies separately, and found that the values of the slope and intercept for the lenticular galaxies are not consistent within the errors with those for the spiral galaxies, but are consistent within the errors with those for the elliptical galaxies. Given this, we conclude that in the $L_{\rm sph} - n_{\rm sph}$ diagram elliptical and lenticular galaxies form together a single (*early-type*) sequence, whereas the combination of lenticular and spiral galaxies do not. Early-type galaxies follow $L_{\rm sph} \propto n_{\rm sph}^{3.60\pm0.19}$; remarkably, this is exactly the same proportionality obtained by Savorgnan et al. (2013) for elliptical galaxies only, upon re-analyzing the dataset from Graham & Guzmán (2003). Late-type galaxies follow a shallower $L_{\rm sph} \propto n_{\rm sph}^{1.44\pm0.52}$ sequence.

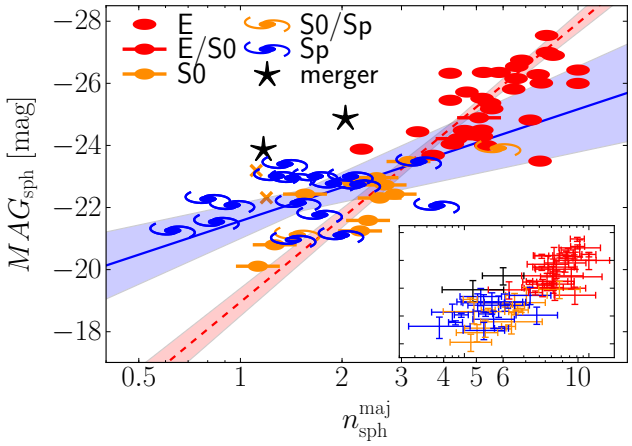

FIG. 1.— Spheroid absolute magnitude (at 3.6 μm) plotted against spheroid Sérsic index measured along the galaxy major-axis. Symbols are coded according to the galaxy morphological type (see legend). The orange crosses denote two lenticular galaxies (NGC 0524 and NGC 3998) which were excluded from the linear regression analysis (see Section 3). The red dashed line indicates the FITEXY bisector linear regression for the $45-2=43$ early-type galaxies (E+S0), with the red shaded area denoting its 1σ uncertainty. The shallower blue solid line shows the FITEXY bisector linear regression for the bulges of the 17 late-type (Sp) galaxies, with the blue shaded area denoting its 1σ uncertainty. The inset panel shows the error bars associated to each data point, where the error bars have the same color coding as the symbols in the main figure.

3.2. $M_{\rm BH} - n_{\rm sph}$

Graham & Scott (2013) presented two different $M_{\rm BH} - L_{\rm sph}$ relations for Sérsic and core-Sérsic spheroids[4] (Graham et al. 2003; Trujillo et al. 2004). However, in *Paper II* we found that the slopes of the $M_{\rm BH} - L_{\rm sph}$ correlations for Sérsic and core-Sérsic spheroids are consistent with each other within their 1σ uncertainties, which prevented us from considering them as two separate sequences. On the other hand, our analysis showed that early- and late-type galaxies follow two different $M_{\rm BH} - L_{\rm sph}$ relations ($M_{\rm BH} \propto L_{\rm sph}^{1.00\pm0.10}$ and $M_{\rm BH} \propto L_{\rm sph}^{2.88\pm0.68}$, respectively). Given that early- and late-type galaxies define two separate sequences in both the $L_{\rm sph} - n_{\rm sph}$ and $M_{\rm BH} - L_{\rm sph}$ diagrams, we investigate substructure in the $M_{\rm BH} - n_{\rm sph}$ diagram. Using the results from the modified FITEXY routine, we find that early-type galaxies follow $M_{\rm BH} \propto n_{\rm sph}^{3.58\pm0.27}$, while late-type galaxies follow $M_{\rm BH} \propto n_{\rm sph}^{4.55\pm0.66}$. The Bayesian estimator `linmix_err` returns consistent results: a slope of 3.44 ± 0.33 for the early-type galaxies and a slope of 4.12 ± 1.07 for the late-type galaxies. In both cases, the values of the slope and intercept for the early- and late-type galaxies are consistent with each other within their 1σ uncertainties[5]. Our analysis shows that the early- and late-type galaxies do not follow two separate trends in the $M_{\rm BH} - n_{\rm sph}$ diagram, i.e. we do not identify any significant substructure based on the galaxy morphological type.

The symmetrical linear regression for all galaxies obtained with the modified FITEXY routine is:

$$\log\left(\frac{M_{\rm BH}}{\rm M_\odot}\right) = (8.15\pm0.06)+(3.37\pm0.15)\left(\log n_{\rm sph}^{\rm maj} - 0.50\right).$$

We have seen that the early- and late-type galaxies in the $M_{\rm BH} - n_{\rm sph}$ diagram can be fit with a single power-law, whereas they follow two separate correlations in the $M_{\rm BH} - L_{\rm sph}$ diagram (*Paper II*). We now want to compare the amount of scatter among these two plots. In Table 5 we summarize the values of the intrinsic scatter in the $M_{\rm BH} - n_{\rm sph}$ and $M_{\rm BH} - L_{\rm sph}$ diagrams for all, early- and late-type galaxies, obtained with the modified FITEXY routine and the Bayesian estimator `linmix_err`. When considering all galaxies, irrespective of their morphological type, the intrinsic scatter of the $M_{\rm BH} - n_{\rm sph}$ relation is smaller than that of the $M_{\rm BH} - L_{\rm sph}$ relation. However, this is obviously not a fair comparison, because of the different nature of the $M_{\rm BH} - n_{\rm sph}$ and $M_{\rm BH} - L_{\rm sph}$ correlations (single and double power-law, respectively). One can obtain more informative results by considering early- and late-type galaxies separately. For the early-type galaxies, the intrinsic scatter of the $M_{\rm BH} - n_{\rm sph}$ relation is consistent[6] with that of the $M_{\rm BH} - L_{\rm sph}$ re-

[4] Core-Sérsic spheroids have partially depleted cores relative to their outer Sérsic light profile, whereas Sérsic spheroids have no central deficit of stars.

[5] In effect, considering the results of the modified FITEXY routine, the slopes of the relations for early- and late-type galaxies are only marginally consistent with each other within their 1σ uncertainties. However, the same slopes obtained with Bayesian estimator `linmix_err` are fully consistent with each other within their 1σ uncertainties.

[6] Looking at the results obtained with the modified FITEXY routine, the values of the intrisic scatter are only marginally consistent with each other, but looking at the results obtained with

lation (within their 1σ uncertainties). For the late-type galaxies, the intrinsic scatter of the $M_{\rm BH} - n_{\rm sph}$ relation is consistent with that of the $M_{\rm BH} - L_{\rm sph}$ relation, except for the inverse $(X|Y)$ regression obtained with the modified FITEXY routine.
In passing, we note that the values of the intrinsic scatter of the $M_{\rm BH} - n_{\rm sph}$ relation are systematically smaller – although consistent within the errors – than the corresponding values of the intrinsic scatter of the $M_{\rm BH} - L_{\rm sph}$ relation. In addition, the values of the intrinsic scatter returned by the modified FITEXY routine are systematically smaller than those output by the Bayesian estimator `linmix_err`.

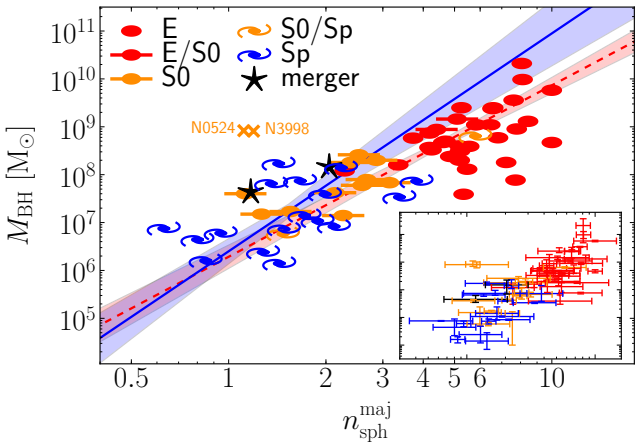

FIG. 2.— Black hole mass plotted against spheroid Sérsic index measured along the galaxy major-axis. Symbols are coded according to the galaxy morphological type (see legend). The orange crosses denote two lenticular galaxies (NGC 0524 and NGC 3998) which were excluded from the linear regression analysis (see Section 3). The red dashed line indicates the FITEXY bisector linear regression for the $45 - 2 = 43$ early-type galaxies (E+S0), with the red shaded area denoting its 1σ uncertainty. The shallower blue solid line shows the FITEXY bisector linear regression for the bulges of the 17 late-type (Sp) galaxies, with the blue shaded area denoting its 1σ uncertainty. The linear regressions for early- and late-type galaxies are consistent with each other within their 1σ uncertainties. The inset panel shows the error bars associated to each data point, where the error bars have the same color coding as the symbols in the main figure.

4. CONCLUSIONS

the Bayesian estimator `linmix_err`, the values of the intrisic scatter are fully consistent with each other.

kkkkk

REFERENCES

Akritas, M. G., & Bershady, M. A. 1996, ApJ, 470, 706
Andredakis, Y. C., Peletier, R. F., & Balcells, M. 1995, MNRAS, 275, 874
Arnold, J. A., Romanowsky, A. J., Brodie, J. P., et al. 2014, ApJ, 791, 80
Beifiori, A., Courteau, S., Corsini, E. M., & Zhu, Y. 2012, MNRAS, 419, 2497
Caon, N., Capaccioli, M., & D'Onofrio, M. 1993, MNRAS, 265, 1013
Cen, R. 2014, ApJ, 790, L24
Emsellem, E., Cappellari, M., Krajnović, D., et al. 2011, MNRAS, 414, 888
Ferrarese, L., & Merritt, D. 2000, ApJ, 539, L9
Gebhardt, K., Bender, R., Bower, G., et al. 2000, ApJ, 539, L13
Graham, A. W. 2001, AJ, 121, 820
Graham, A. W., & Driver, S. P. 2005, PASA, 22, 118
—. 2007, ApJ, 655, 77
Graham, A. W., Erwin, P., Trujillo, I., & Asensio Ramos, A. 2003, AJ, 125, 2951
Graham, A. W., & Guzmán, R. 2003, AJ, 125, 2936
Graham, A. W., & Scott, N. 2013, ApJ, 764, 151
Graham, A. W., & Worley, C. C. 2008, MNRAS, 388, 1708
Iodice, E., D'Onofrio, M., & Capaccioli, M. 1997, in Astronomical Society of the Pacific Conference Series, Vol. 116, The Nature of Elliptical Galaxies; 2nd Stromlo Symposium, ed. M. Arnaboldi, G. S. Da Costa, & P. Saha, 84
Iodice, E., D'Onofrio, M., & Capaccioli, M. 1999, in Astronomical Society of the Pacific Conference Series, Vol. 176, Observational Cosmology: The Development of Galaxy Systems, ed. G. Giuricin, M. Mezzetti, & P. Salucci, 402
Jerjen, H., Binggeli, B., & Freeman, K. C. 2000, AJ, 119, 593
Kelly, B. C. 2007, ApJ, 665, 1489
Khosroshahi, H. G., Wadadekar, Y., & Kembhavi, A. 2000, ApJ, 533, 162
Magorrian, J., Tremaine, S., Richstone, D., et al. 1998, AJ, 115, 2285
Nipoti, C. 2015, ApJ, 805, L16

TABLE 2
Linear regression analysis of the $L_{\rm sph} - n_{\rm sph}$ diagram.

Subsample (size)	**Regression**	$\boldsymbol{\alpha}$	$\boldsymbol{\beta}$	$\langle \log n_{\rm sph}^{\rm maj} \rangle$	$\boldsymbol{\epsilon}$	$\boldsymbol{\Delta}$
	$MAG_{\rm sph}/[\rm mag] = \alpha + \beta\big(\log n_{\rm sph}^{\rm maj} - \langle \log n_{\rm sph}^{\rm maj} \rangle\big)$					
All (64)	BCES $(Y\|X)$	-23.89 ± 0.15	-6.90 ± 0.74	0.50	–	1.22
	mFITEXY $(Y\|X)$	-23.91 ± 0.13	-6.63 ± 0.45	0.50	$0.59^{+0.16}_{-0.11}$	1.01
	`linmix_err` $(Y\|X)$	-23.89 ± 0.14	-6.34 ± 0.57	0.50	0.74 ± 0.13	1.14
	BCES $(X\|Y)$	-23.89 ± 0.15	-6.75 ± 0.52	0.50	–	1.20
	mFITEXY $(X\|Y)$	-23.89 ± 0.14	-7.49 ± 0.53	0.50	$0.62^{+0.18}_{-0.12}$	1.32
	`linmix_err` $(X\|Y)$	-23.90 ± 0.16	-7.49 ± 0.62	0.50	0.80 ± 0.16	1.32
	BCES Bisector	-23.89 ± 0.15	-6.83 ± 0.58	0.50	–	1.21
	mFITEXY Bisector	-23.90 ± 0.13	-7.04 ± 0.35	0.50	–	1.24
	`linmix_err` Bisector	-23.89 ± 0.15	-6.87 ± 0.42	0.50	–	1.21
Elliptical (E) (30)	BCES $(Y\|X)$	-25.46 ± 1.12	38.47 ± 114.45	0.76	–	6.37
	mFITEXY $(Y\|X)$	-25.74 ± 0.18	-9.74 ± 1.59	0.76	$0.24^{+0.32}_{-0.24}$	0.94
	`linmix_err` $(Y\|X)$	-25.65 ± 0.21	-7.87 ± 2.15	0.76	0.61 ± 0.22	1.06
	BCES $(X\|Y)$	-25.46 ± 0.23	-10.73 ± 3.21	0.76	–	1.29
	mFITEXY $(X\|Y)$	-25.74 ± 0.20	-10.42 ± 1.79	0.76	$0.22^{+0.38}_{-0.22}$	1.29
	`linmix_err` $(X\|Y)$	-25.72 ± 0.28	-10.92 ± 2.70	0.76	0.73 ± 0.34	1.33
	BCES Bisector	-25.46 ± 0.20	0.03 ± 0.05	0.76	–	1.14
	mFITEXY Bisector	-25.74 ± 0.19	-10.07 ± 1.19	0.76	–	1.26
	`linmix_err` Bisector	-25.68 ± 0.25	-9.15 ± 1.74	0.76	–	1.16
Lenticular (S0) (11)	BCES $(Y\|X)$	-22.08 ± 1.66	33.52 ± 98.87	0.33	–	6.09
	mFITEXY $(Y\|X)$	-22.11 ± 0.24	-6.31 ± 2.45	0.33	$0.42^{+0.28}_{-0.17}$	0.71
	`linmix_err` $(Y\|X)$			0.33		
	BCES $(X\|Y)$	-22.08 ± 0.19	-6.83 ± 1.16	0.33	–	0.71
	mFITEXY $(X\|Y)$	-21.94 ± 0.44	-13.16 ± 7.91	0.33	$0.61^{+0.60}_{-0.56}$	1.39
	`linmix_err` $(X\|Y)$			0.33		
	BCES Bisector	-22.08 ± 0.30	0.06 ± 0.05	0.33	–	1.09
	mFITEXY Bisector	-22.05 ± 0.35	-8.55 ± 2.79	0.33	–	0.84
	`linmix_err` Bisector			0.33	–	
Spiral (Sp) (17)	BCES $(Y\|X)$	-22.33 ± 0.26	-5.31 ± 5.83	0.18	–	1.15
	mFITEXY $(Y\|X)$	-22.22 ± 0.19	-2.17 ± 0.98	0.18	$0.53^{+0.24}_{-0.13}$	0.72
	`linmix_err` $(Y\|X)$	-22.26 ± 0.24	-1.53 ± 1.88	0.18	0.71 ± 0.22	0.78
	BCES $(X\|Y)$	-22.33 ± 0.26	-5.19 ± 3.77	0.18	–	1.13
	mFITEXY $(X\|Y)$	-22.28 ± 0.44	-9.08 ± 5.31	0.51	$1.12^{+0.54}_{-0.31}$	1.83
	`linmix_err` $(X\|Y)$	-22.24 ± 0.71	-11.12 ± 13.59	0.18	1.95 ± 2.47	2.24
	BCES Bisector	-22.33 ± 0.26	-5.25 ± 3.38	0.18	–	1.14
	mFITEXY Bisector	-22.23 ± 0.33	-3.60 ± 1.29	0.18	–	0.92
	`linmix_err` Bisector	-22.25 ± 0.53	-2.88 ± 2.66	0.18	–	0.84

Press, W. H., Teukolsky, S. A., Vetterling, W. T., & Flannery, B. P. 1992, Numerical recipes in FORTRAN. The art of scientific computing

Rusli, S. P., Erwin, P., Saglia, R. P., et al. 2013, AJ, 146, 160

Sani, E., Marconi, A., Hunt, L. K., & Risaliti, G. 2011, MNRAS, 413, 1479

Savorgnan, G., Graham, A. W., Marconi, A., et al. 2013, MNRAS, 434, 387

Scott, N., Davies, R. L., Houghton, R. C. W., et al. 2014, MNRAS, 441, 274

Seigar, M. S., & James, P. A. 1998, MNRAS, 299, 672

Sérsic, J. L. 1963, Boletin de la Asociacion Argentina de Astronomia La Plata Argentina, 6, 41

—. 1968, Atlas de galaxias australes

Sheth, K., Regan, M., Hinz, J. L., et al. 2010, PASP, 122, 1397

Tremaine, S., Gebhardt, K., Bender, R., et al. 2002, ApJ, 574, 740

Trujillo, I., Erwin, P., Asensio Ramos, A., & Graham, A. W. 2004, AJ, 127, 1917

Vika, M., Driver, S. P., Cameron, E., Kelvin, L., & Robotham, A. 2012, MNRAS, 419, 2264

Young, C. K., & Currie, M. J. 1994, MNRAS, 268, L11

TABLE 3
LINEAR REGRESSION ANALYSIS OF THE $L_{\rm sph} - n_{\rm sph}$ DIAGRAM.

Subsample (size)	**Regression**	$\boldsymbol{\alpha}$	$\boldsymbol{\beta}$	$\langle \log n_{\rm sph}^{\rm maj} \rangle$	$\boldsymbol{\epsilon}$	$\boldsymbol{\Delta}$
Early-type (E+S0) (43)	BCES $(Y\|X)$	-24.55 ± 0.22	-11.84 ± 2.29	0.64	–	1.50
	mFITEXY $(Y\|X)$	-24.74 ± 0.14	-8.86 ± 0.66	0.51	$0.27^{+0.20}_{-0.27}$	0.87
	`linmix_err` $(Y\|X)$	-24.70 ± 0.17	-8.28 ± 0.87	0.64	0.58 ± 0.17	0.98
	BCES $(X\|Y)$	-24.55 ± 0.14	-8.25 ± 0.63	0.64	–	0.96
	mFITEXY $(X\|Y)$	-24.74 ± 0.14	-9.13 ± 0.68	0.64	$0.23^{+0.25}_{-0.23}$	1.08
	`linmix_err` $(X\|Y)$	-24.73 ± 0.18	-9.08 ± 0.87	0.64	0.60 ± 0.21	1.07
	BCES Bisector	-24.55 ± 0.17	-9.73 ± 1.05	0.64	–	1.14
	mFITEXY Bisector	-24.74 ± 0.14	-8.99 ± 0.48	0.64	–	1.06
	`linmix_err` Bisector	-24.72 ± 0.17	-8.66 ± 0.63	0.64	–	1.02
Bulge (S0+Sp) (30)	BCES $(Y\|X)$	-22.25 ± 0.20	-5.88 ± 3.06	0.26	–	1.16
	mFITEXY $(Y\|X)$	-22.19 ± 0.14	-2.99 ± 0.73	0.26	$0.52^{+0.18}_{-0.10}$	0.75
	`linmix_err` $(Y\|X)$	-22.20 ± 0.17	-2.48 ± 1.21	0.26	0.67 ± 0.15	0.83
	BCES $(X\|Y)$	-22.25 ± 0.20	-5.85 ± 1.83	0.26	–	1.15
	mFITEXY $(X\|Y)$	-22.17 ± 0.25	-7.65 ± 2.43	0.26	$0.87^{+0.30}_{-0.18}$	1.46
	`linmix_err` $(X\|Y)$	-22.16 ± 0.31	-7.80 ± 3.89	0.26	1.18 ± 0.65	1.48
	BCES Bisector	-22.25 ± 0.20	-5.87 ± 2.06	0.26	–	1.16
	mFITEXY Bisector	-22.18 ± 0.20	-4.34 ± 0.84	0.26	–	0.96
	`linmix_err` Bisector	-22.19 ± 0.25	-3.83 ± 1.39	0.26	–	0.91

NOTE. — For each subsample, we indicate $\langle \log n_{\rm sph} \rangle$, its average value of spheroid Sérsic index. In the last two columns, we report ϵ, the intrinsic scatter, and Δ, the total rms scatter in the $L_{\rm sph}$ direction. The lenticular galaxies NGC 0524 and NGC 3998 were excluded from the linear regression analysis (see Section 3). Both the early- and late-type subsamples do not contain the two galaxies classified as S0/Sp and the two galaxies classified as mergers (45+17=66-2-2).

TABLE 4
LINEAR REGRESSION ANALYSIS OF THE $M_{\rm BH} - n_{\rm sph}$ DIAGRAM.

Subsample (size)	**Regression**	$\boldsymbol{\alpha}$	$\boldsymbol{\beta}$	$\langle \log n_{\rm sph}^{\rm maj} \rangle$	$\boldsymbol{\epsilon}$	$\boldsymbol{\Delta}$
	$\log(M_{\rm BH}/[{\rm M}_\odot]) = \alpha + \beta(\log n_{\rm sph}^{\rm maj} - \langle \log n_{\rm sph}^{\rm maj} \rangle)$					
All (64)	BCES $(Y\|X)$	8.14 ± 0.07	3.49 ± 0.36	0.50	–	0.61
	mFITEXY $(Y\|X)$	8.15 ± 0.06	3.26 ± 0.21	0.50	$0.22^{+0.10}_{-0.07}$	0.46
	`linmix_err` $(Y\|X)$	8.15 ± 0.06	3.17 ± 0.24	0.50	0.28 ± 0.07	0.56
	BCES $(X\|Y)$	8.14 ± 0.08	3.52 ± 0.25	0.50	–	0.61
	mFITEXY $(X\|Y)$	8.15 ± 0.06	3.49 ± 0.23	0.50	$0.23^{+0.10}_{-0.07}$	0.61
	`linmix_err` $(X\|Y)$	8.15 ± 0.07	3.49 ± 0.26	0.50	0.29 ± 0.08	0.61
	BCES Bisector	8.14 ± 0.07	3.51 ± 0.28	0.50	–	0.61
	mFITEXY Bisector	8.15 ± 0.06	3.37 ± 0.15	0.50	–	0.59
	`linmix_err` Bisector	8.15 ± 0.07	3.32 ± 0.18	0.50	–	0.58
Early-type (E+S0) (43)	BCES $(Y\|X)$	8.54 ± 0.10	4.07 ± 0.87	0.64	–	0.65
	mFITEXY $(Y\|X)$	8.58 ± 0.07	3.32 ± 0.34	0.64	$0.24^{+0.10}_{-0.07}$	0.45
	`linmix_err` $(Y\|X)$	8.57 ± 0.08	3.12 ± 0.43	0.64	0.32 ± 0.08	0.53
	BCES $(X\|Y)$	8.54 ± 0.09	3.95 ± 0.55	0.64	–	0.63
	mFITEXY $(X\|Y)$	8.59 ± 0.08	3.88 ± 0.43	0.64	$0.26^{+0.11}_{-0.08}$	0.62
	`linmix_err` $(X\|Y)$	8.59 ± 0.09	3.82 ± 0.50	0.64	0.35 ± 0.10	0.61
	BCES Bisector	8.54 ± 0.10	4.01 ± 0.63	0.64	–	0.64
	mFITEXY Bisector	8.59 ± 0.07	3.58 ± 0.27	0.64	–	0.58
	`linmix_err` Bisector	8.58 ± 0.08	3.44 ± 0.33	0.64	–	0.56
Spiral (Sp) (17)	BCES $(Y\|X)$	7.18 ± 0.28	6.78 ± 6.62	0.18	–	1.23
	mFITEXY $(Y\|X)$	7.24 ± 0.13	4.48 ± 0.90	0.18	$0.13^{+0.42}_{-0.13}$	0.52
	`linmix_err` $(Y\|X)$	7.22 ± 0.16	3.57 ± 1.36	0.18	0.39 ± 0.19	0.70
	BCES $(X\|Y)$	7.18 ± 0.23	5.48 ± 1.93	0.18	–	0.99
	mFITEXY $(X\|Y)$	7.24 ± 0.14	4.62 ± 0.96	0.18	$0.13^{+0.43}_{-0.13}$	0.85
	`linmix_err` $(X\|Y)$	7.21 ± 0.21	4.86 ± 1.64	0.18	0.45 ± 0.31	0.89
	BCES Bisector	7.18 ± 0.25	6.06 ± 3.66	0.18	–	1.10
	mFITEXY Bisector	7.24 ± 0.14	4.55 ± 0.66	0.18	–	0.84
	`linmix_err` Bisector	7.22 ± 0.19	4.12 ± 1.07	0.18	–	0.77

NOTE. — For each subsample, we indicate $\langle \log n_{\rm sph} \rangle$, its average value of spheroid Sérsic index. In the last two columns, we report ϵ, the intrinsic scatter, and Δ, the total rms scatter in the $L_{\rm sph}$ direction. The lenticular galaxies NGC 0524 and NGC 3998 were excluded from the linear regression analysis (see Section 3). Both the early- and late-type subsamples do not contain the two galaxies classified as S0/Sp and the two galaxies classified as mergers (45+17=66-2-2).

TABLE 5
INTRINSIC SCATTER OF THE $M_{\rm BH} - n_{\rm sph}$ AND $M_{\rm BH} - L_{\rm sph}$ RELATIONS.

Subsample	**Regression**	$\boldsymbol{\epsilon}$ **for** $\boldsymbol{M_{\rm BH} - n_{\rm sph}}$	$\boldsymbol{\epsilon}$ **for** $\boldsymbol{M_{\rm BH} - L_{\rm sph}}$
All	mFITEXY $(Y\|X)$	$0.22^{+0.10}_{-0.07}$	$0.49^{+0.06}_{-0.05}$
	`linmix_err` $(Y\|X)$	0.29 ± 0.07	0.51 ± 0.06
	mFITEXY $(X\|Y)$	$0.23^{+0.10}_{-0.07}$	$0.58^{+0.07}_{-0.06}$
	`linmix_err` $(X\|Y)$	0.30 ± 0.07	0.60 ± 0.09
Early-type	mFITEXY $(Y\|X)$	$0.24^{+0.10}_{-0.07}$	$0.40^{+0.06}_{-0.05}$
	`linmix_err` $(Y\|X)$	0.32 ± 0.08	0.41 ± 0.06
	mFITEXY $(X\|Y)$	$0.26^{+0.11}_{-0.08}$	$0.49^{+0.08}_{-0.06}$
	`linmix_err` $(X\|Y)$	0.35 ± 0.10	0.51 ± 0.10
Late-type	mFITEXY $(Y\|X)$	$0.13^{+0.42}_{-0.13}$	$0.55^{+0.15}_{-0.10}$
	`linmix_err` $(Y\|X)$	0.39 ± 0.19	0.63 ± 0.16
	mFITEXY $(X\|Y)$	$0.13^{+0.43}_{-0.13}$	$1.09^{+0.41}_{-0.24}$
	`linmix_err` $(X\|Y)$	0.45 ± 0.31	1.31 ± 0.97